PCIM Europe 2018; International Exhibition and Conference for Power Electronics, Intelligent Motion, Renewable Energy and Energy Management; Proceedings of

Power Supply System with Integrated Energy Storage for Superconducting Magnets

M. Papamichali, E.Coulinge, F. Freijedo, *et al.*

POWER ELECTRONICS LABORATORY
ÉCOLE POLYTECHNIQUE FÉDÉRALE DE LAUSANNE

Power Supply System with Integrated Energy Storage for Superconducting Magnets

Maria Papamichali, Emilien Coulinge, Francisco D. Freijedo, Dražen Dujić
Power Electronics Laboratory, École Polytechnique Fédérale de Lausanne (EPFL), Switzerland
maria.papamichali@epfl.ch, emilien.coulinge@epfl.ch
francisco.freijedo@epfl.ch, drazen.dujic@epfl.ch

Abstract

To achieve higher collision rate of particle beams, CERN Large Hadron Collider requires new superconducting magnets and associated power supplies at the interaction points for its High-Luminosity upgrade. A new family of two-quadrant converters with integrated energy storage is studied in order to increase the system availability and energy efficiency. This paper describes topological implementation with an energy storage solution based on supercapacitor, considering real operating cycle and superconducting magnet parameters. Power supply control and energy management considerations are presented and verified through simulations of a complete system, providing insight for the future design of the system.

1. Introduction

The upgrade of Large Hadron Collider (LHC) to High-Luminosity LHC (HL-LHC) scheduled for mid 2020's requires stronger superconducting magnets, producing a magnetic field up to $11\,\mathrm{T}$ for the final focusing of the particle beams prior to collision at the interaction points [1]. Furthermore, a new system infrastructure places the associated power supplies in an underground technical gallery in order to ease the connection to the superconducting link that minimizes the length of the DC water-cooled cables at the output of the power supply. Only this portion of DC cables will define the resistance of the system towards the superconducting magnets and, as a result, the resistance value of the load is greatly reduced, to less than $1\,\mathrm{m\Omega}$ [2]. Based on the presently used 1-Quadrant (1Q) main power supplies, the consequent increase of the load time constant would lead to ramp-down (RD) time well above the operational requirements [3], where the free-wheeling decrease of the current in the Inner-Triplet magnet (ITM) is done through dissipation in the resistance of the cable

The foreseen superconducting magnet operating cycle is defined as a sequence of three distinct operating modes. The current is increased during the 20-minute ramp-up (RU) with a slope defined by the operation requirements ($16\,\mathrm{A/s}$). Then, the magnet current is tightly regulated during the flat-top (FT) process within 8 to 16 hours at the rated value of $18\,\mathrm{kA}$ to achieve normal beam operation. After the beam is dumped, the magnet current must be decreased in 20 minutes during RD in order to prepare the system for the next experimental cycle.

The goal of the HL-LHC upgrade is to achieve the aforementioned operating cycle via a 2-Quadrant (2Q) power supply [4], thanks to which the voltage across the load can be reversed during RD phase, leading to a controlled energy recovery from the energy stored in the superconducting magnet. Only the high-current output stage [5] will provide the 2Q characteristic of the supply which allows the energy recovered to be used in the next RU. Therefore, the power drawn from the grid is reduced as well as the rating of the input stage. This paper discusses such a scenario considering Supercapacitor (SC) as integrated energy storage system for the energy recovery.

The structure of this paper is organised as follows: in Section 2 the general description of the future main power supply configuration is described; Section 3, the integration of SC technology in the system is discussed; then, the control strategy of the controllable converters and the Energy Management Unit (EMU) are presented, followed by Section 5 and 6 which contain the simulation results and discussion.

ISBN 978-3-8007-4646-0

2. System description

The concept of the analysed power supply configuration is shown in Fig. 1a. It is composed of an input stage consisting of a 3-Phase Diode Rectifier (3P DR) followed by a Phase-Shift Full-Bridge converter (PS FB) providing galvanic isolation and an output 2Q converter stage connected to the superconducting magnet. The latter, rated at [$18\,\mathrm{kA}$, $\pm 10\,\mathrm{V}$], interfaces the integrated Energy Storage Unit (ESU) with the RL-load of constant value. The pure inductance and resistance correspond to the ITM and DC cables, respectively [6].

The load-cycle is described in Fig. 2a and defines the requirements for the desired power-flow, which is key for the control of the power supply. During RU phase, as shown in Fig. 2b, the power losses of the resistive part of the load are supplied by the grid and (reactive) energy is provided to the ITM by the ESU. During FT the grid provides the resistive power demand of the load due to losses associated with DC cables and overall converter losses, which are neglected in the present analysis. The ITM current is tightly regulated at $18\,\mathrm{kA}$ within an error-band of $1\,\mathrm{ppm}$, as it directly impacts the quality of particle beams at collision. Finally, during RD, the current through the load gradually decreases and the magnetic energy of the ITM is recovered by the ESU increasing its state-of-charge (SoC) without any participation from the grid-side converter. At the end of the cycle, the SoC does not reach 100%, as part of the energy is lost due to Joule effect in the resistive part of the system load. The unidirectional grid-side converter covers the remaining SoC of the ESU before the initiation of the next cycle of the LHC.

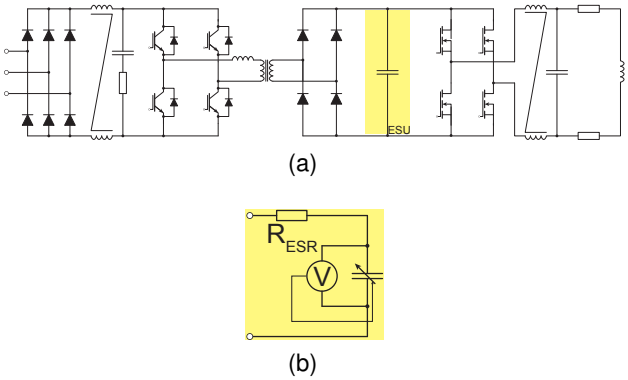

Fig. 1: (a) Simplified circuit of the power supply system; (b) Supercapacitor model used for simulations.

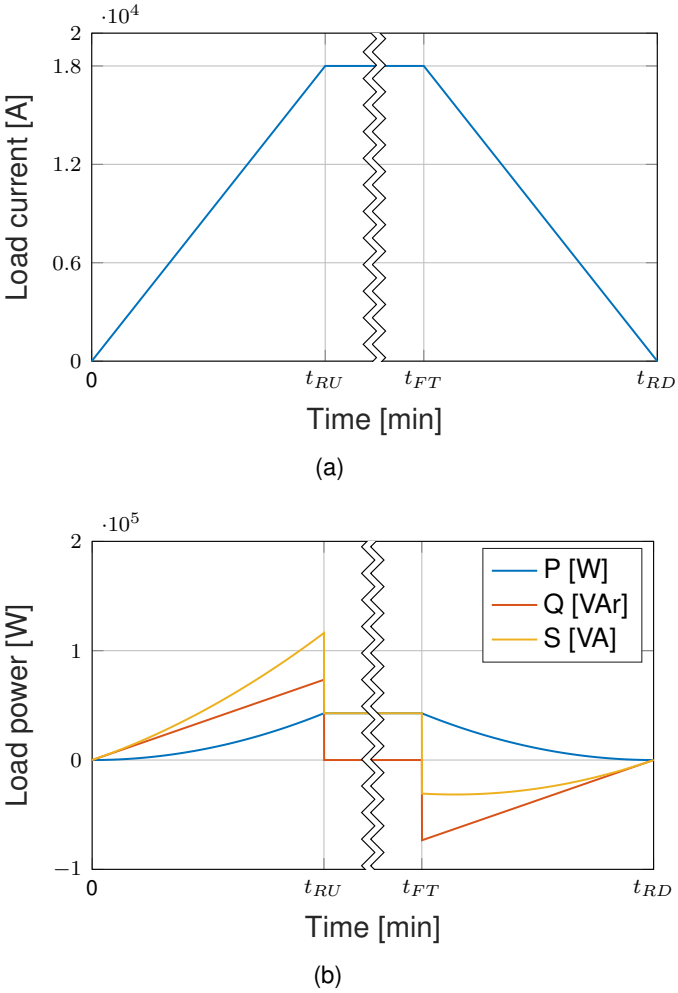

Fig. 2: Load-cycle: (a) current through the ITM, t_{RU} corresponds to the RU process duration, $t_{FT} - t_{RU}$ to the FT and $t_{RD} - t_{FT}$ to the RD duration; (b) load requirements: during the RU the active and reactive power requirements increase, as the current through the ITM increases. During FT grid-side converter provides only active power to cover losses in the system. During the RD, the apparent power of the load is negative meaning that energy is returned to the ESU.

3. Supercapacitor as ESU

The different possible implementations of ESU generate several design solutions discussed in [4]. In this paper, the ESU is installed in the main power-flow path, on the low voltage side connected back-to-back with the 2Q converter.

Suitable energy storage technologies considered are batteries and SC. Battery candidates are superior in terms of weight and volume by factors of 8.5 and 14, respectively [7]. However, the battery

ISBN 978-3-8007-4646-0

charging current profile during RD, as well as the tight time-frame of this process pose challenges. Moreover, the exceptional cycle lifetime of SC technology brings makes this solution compatible to the system lifetime expectancy of 200 days of yearly operation over the next 20 years. Presently, the SC technology is considered as ESU, sized according to the energy requirements of the ITM [7].

The control of the system is designed to operate the SC with an input voltage range from full to half-rated SC voltage, achieving 75% extraction of its energy content. The SC model considers an Equivalent Series Resistance (ESR) and a voltage dependent capacitance according to the linear law $C(V) = C_0 + k \cdot V$, where C_0 is a base capacitance at zero voltage and k is the slope of the function [8]. The supercapacitor model is shown in Fig. 1b [9]. The present sizing is performed for rated voltage $24\,\mathrm{V}$ and based on real SC cell products arranged in series and in parallel, in order to achieve the voltage and energy requirement. The evolution of the SC voltage can be seen in Fig. 3a. The resulting SC capacitance for the voltage range $[12, 24]\ \mathrm{V}$ is in the range $[19, 23]\ \mathrm{kF}$ and is shown in Fig. 3b.

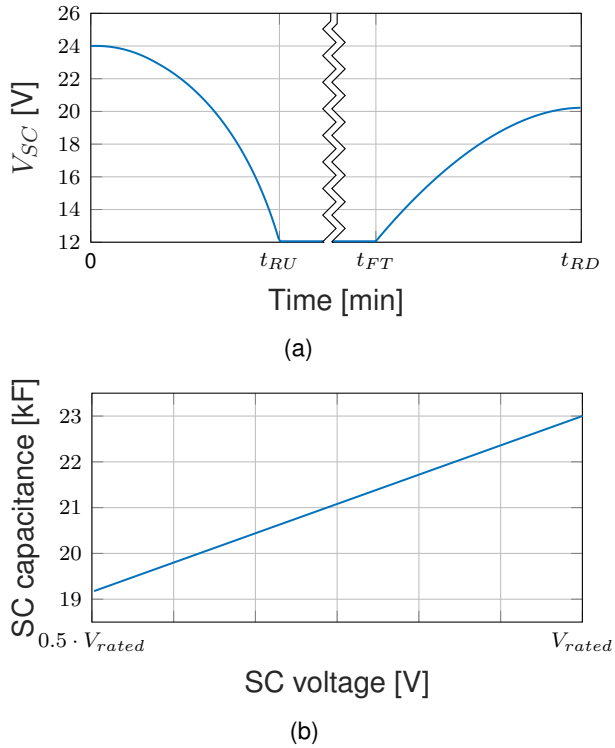

Fig. 3: (a) SC voltage in one simulated cycle; (b) the range of the voltage dependent capacitance.

4. Control strategy

From the system architecture, the controlled variables are the voltage across the SC regulated by the PS FB and the superconducting magnet current through the 2Q output DC-DC stage. The switching and sampling frequency is considered as $f_{sw} = 5\,\mathrm{kHz}$. The EMU is the high-level strategy coordinating the controllers in order to achieve the correct assignment of power delivery tasks and, hence, the desired power-flow strategy.

The PS FB output voltage is a function of the duty cycle and the transformer turns ratio, which adjusts the 3P DR output voltage to the operating voltage range of the SC. The outer voltage loop regulates the SC voltage in accordance to references from the inner current loop, driven by references provided by EMU as shown in Fig. 4a. Saturation blocks accompanied by anti-windup ensure that the inner loop respects the rating of the input stage and the outer loop the operating voltage range of SC. The gains of the cascaded loop and anti-windup are shown in Table 1, where subscript i indicates inner current loop and v outer voltage loop. The high order of magnitude in outer loop gains is due to the high-value capacitance of the SC. Therefore, during FT, any increase of the voltage across the SC should be requested in the form of low-slope ramp, in order to avoid controller saturation.

As far as the output stage DC-DC converter is concerned, its goal is to control the current through

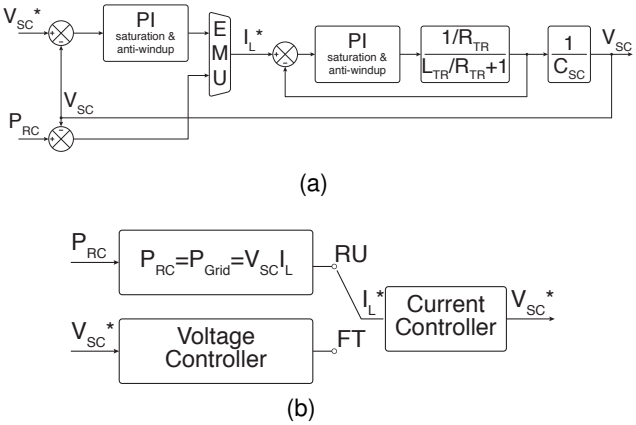

Fig. 4: (a) Simplified control loop scheme; (b) Control modes for ramp-up and flat-top.

ISBN 978-3-8007-4646-0

Table 1: Gains of the PI control loops and anti-windup of the cascaded PS FB control design.

Inner loop PI_i			**Outer loop** PI_v		
$k_{p,i}$	$k_{i,i}$	$k_{awu,i}$	$k_{p,v}$	$k_{i,v}$	$k_{awu,v}$
0.035	1.667	47.6	$3.5 \cdot 10^6$	$2.9 \cdot 10^8$	83.3

Table 2: Gains of the PI control loops and anti-windup of the DC/DC converter control design. The subscript l stands for $load$.

Load current loop PI_l			
Case	k_{p_l}	k_{i_l}	k_{awu_l}
Conservative	$15.3 \cdot 10^3$	15.84	0.001
Optimistic	$15.3 \cdot 10^3$	7.92	0.0005

Table 3: Load specifications for conservative and optimistic case used in the DC-DC control loop gains computation and simulation results.

Case	L_M $[mH]$	R_C $[m\Omega]$	Time constant τ [min]
Conservative	255	0.264	16
Optimistic	255	0.132	32

the load comprised by cable resistance (R_C) and ITM inductance (L_M). For this reason, only a current loop is implemented accompanied by saturation and anti-windup blocks, while unipolar modulation generates the PWM signals. The resulting control gains can be seen in Table 2. In this study, the gain calculation and simulations are performed based on two load cases, resulting in different resistances to be considered. The comparison is performed at the level of cable length, therefore resistive part of the load, which would lead to different energy recovery capabilities. A conservative scenario considers the cable resistance of a $38\,\mathrm{m}$ wire with $2600\,\mathrm{mm}^2$ section, while an optimistic one minimizes the cable length, i.e. $16\,\mathrm{m}$ wire of the same section. The load specifications, that are used for the simulation studies are summarized in Table 3, and may not actually represent the final design.

At system level, the PS FB and the DC-DC converters are connected back-to-back with the SC as a DC-link. The DC-DC current control operates always in single-mode, as described previously. However, the control of the voltage across the SC, which is the key to achieve the desired power-flow strategy is achieved by means of two different control modes. The EMU is responsible for the correct share of drawn power between the grid-side (active power) and the SC (reactive power). The power losses of the resistive part of the load (P_{R_C}) is foreseen to be covered by the grid-side, calculated as $P_{R_C} = V_{R_C} \cdot I_{OUT}$, where V_{R_C} is the voltage across the resistance of the cables and I_{OUT} is the load current.

The EMU decides the source of reference current of the inner current control loop of the PS FB control, according to the mode of operational cycle, as shown in Fig. 4b. During RU the controlled reduction of the SC voltage in order to supply energy to the superconducting magnet is not performed through the cascaded mode of PS FB: the outer voltage controller is deactivated. It is rather achieved indirectly by imposing to the grid-side to feed the power losses of the load by suitable references on the inner current controller, i.e. reference current through the series inductance of the transformer secondary winding (I_L^*). This is calculated through the active power demanded by the resistive part of the load divided by the updated decreasing SC voltage due to the reactive power intake of the supeconducting magnet, therefore $I_L^* = \frac{P_{R_C}}{V_{SC}}$. At the end of the RU process, the voltage across the SC has reached a level, such that its specified useful energy has been delivered to the load.

During FT, the reactive requirements of the load are zero and only active power is requested. The target is to provide this power from PS FB and not by the SC. Thus the voltage across the SC is controlled in such a way to follows a desired value (either a constant or an increasing value) in order to re-establish the SoC at desired value. At this stage, the voltage controller of the cascade controller is activated and the reference current of the inner current controller is provided by it. At the transition between RU and FT processes, the shift between the two control modes is smoothly performed by setting as reference of the outer voltage loop the SC voltage value measured exactly at end of the RU process.

During the RD, as long as the load voltage is positive, power is delivered by the grid-side and the PS FB converter adjusts the duty cycle in order

to achieve the reduction of the current through the secondary winding of the transformer. Once the load voltage becomes negative, the grid-side does not participate, since it is a uni-directional stage. Therefore, energy is returned to the SC and as a result, the voltage across it increases according to the energy received, which is less than what was delivered during the RU, due to the power loss in the resistive part of the load. No regulation is in reality needed, since the only energy path is that between the superconducting magnet and the SC. With knowledge of losses in the system, SC initial SoC (at the end of FT) and final SoC (at the end of RD) can be adjusted, depending on the implemented EMU strategy.

5. Simulation results

Switched PLECS simulations were performed, with focus being on the energy management during typical operating cycle. The resistive part of the load is the only responsible for the power consumption seen from the grid side. Assuming the optimistic load case scenario, as presented in Table 3, the power sharing is shown in Fig. 5a. As may be seen, during RU and FT load active power needs are provided by grid-side (P_{GS}), while during RD grid-side is not active. The SC (Q_{SC}) provides the load reactive power needs during RU and the magnetic energy of the load is transferred to the SC during RD. Therefore, the power-flow strategy is executed correctly and the energy storage system based on SC is providing adequate support.

Energy-wise, Fig. 5b shows the effect on the energy recovery at the end of the cycle by comparing the optimistic against conservative load case scenario. Considering the magnetic energy required by the ITM as $E_{ITM} = {}^1\!/_2 \cdot L \cdot I^2 = 40\,\mathrm{MJ}$, the energy recovery in the former case is $25.1\,\mathrm{MJ}$, which represents the 62.5% while in the latter case only $8.8\,\mathrm{MJ}$, i.e. 22% can be recovered. Obviously, energy recovery will be further reduced if power converter losses are considered. As a consequence, the role of the grid-side during the FT process is indispensable for the increase of SoC of the SC and its preparation for the next cycle.

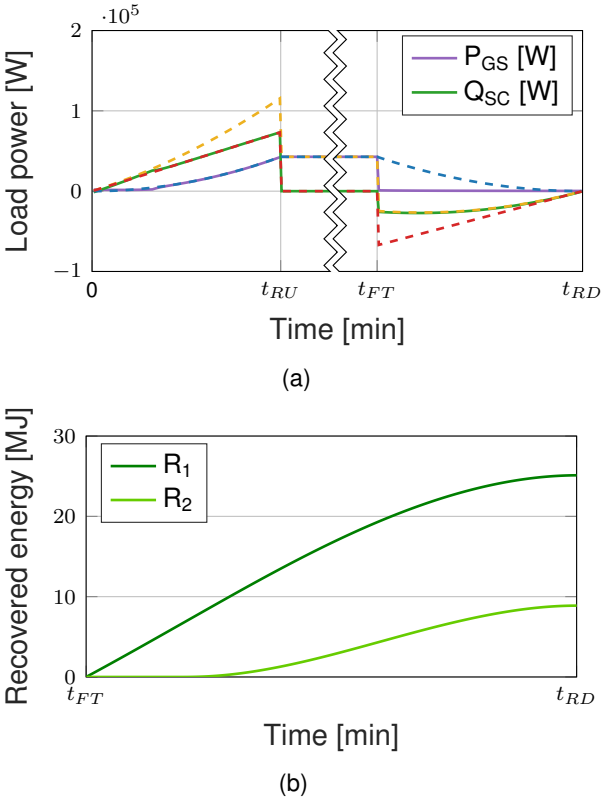

Fig. 5: Power-flow strategy: (a) the discontinuous lines correspond to the load power graphs shown in Fig. 2b. (b) the energy recovery at the SC level during the RD process is sensitive to resistive part of supplying cables. As observed, for higher resistance values, the energy recovery does not start immediately, but only after the load voltage becomes negative.

6. Conclusions

This paper discusses the integration of ESU in the 2Q superconducting magnet power supply, foreseen for the future upgrade of LHC to HL-LHC. Simplified converter implementation is used to explore SC based energy storage. Analysed power-flow strategy considers the delivery of the active power from the grid-side during the RU and FT processes, and use of SC to ramp-up the current of superconducting magnets. The energy stored in the superconducting magnet is recovered by the SC during RD, rather than being completely dissipated as Joule losses. Simulation results highlight the importance and impact of the cable resistances on the overall energy recovery potentials. Further detailed system studies are required to asses the overall viability and performances of the ESU integration.

ISBN 978-3-8007-4646-0

References

[1] G. Apollinari, I. Béjar Alonso, O. Brüning, M. Lamont, and L. Rossi, *High-Luminosity Large Hadron Collider (HL-LHC)*, December. 2015, vol. 4.

[2] O. Brüning, M. Lamont, L. Rossi, and L. Tavian, "High-Luminosity Large Hadron Collider, Technical Design Report V0.1," 2017.

[3] S. Yammine and H. Thiesen, "HL-LHC Inner-Triplet Powering and Control Strategy," in *IPAC2017*, 2017, pp. 3544–3546.

[4] E. Coulinge, D. Dujic, and J.-P. Burnet, "High-Current Low-Voltage Power Supplies for Superconducting Magnet," in *19th International Symposium on Power Electronics*, 2017.

[5] E. Coulinge, D. Dujic, J.-P. Burnet, and S. Pittet, "Comparative Study of Two-Quadrant DC/DC Stage in Power Supply for Superconducting Magnets," in *19th International Conference on Industrial Technology*, 2018.

[6] F. Bordry, D. Nisbet, H. Thiesen, and J. Thomsen, "Powering and Control Strategy for the Main Quadrupole Magnets of the LHC Inner-Triplet System," *Power Electronics and Applications, 2009. EPE'09.*, pp. 1–10, 2009.

[7] M. Papamichali, "Superconducting Magnet Power Supply With Integrated Energy Storage," *Master Thesis, EPFL, Lausanne, September 2017*, 2017.

[8] P. J. Grbovic, *Ultra-capacitors in power conversion systems: analysis, modeling and design in theory and practice*. Wiley - IEEE, 2014.

[9] J. Schönberger, "Modeling a Supercapacitor using PLECS," *Plexim GmbH, version*, pp. 1–6, 2010.

ISBN 978-3-8007-4646-0